High-Resolution Method for Primary Signal Processing in HFSWR

Dragan Golubović
University of Belgrade,
School of Electrical Engineering
Vlatacom Institute
Belgrade, Serbia
dragan.golubovic@vlatacom.com

Miljko Erić
Vlatacom Institute
University of Belgrade,
School of Electrical Engineering
Belgrade, Serbia
miljko.eric@vlatacom.com

Nenad Vukmirović
University of Belgrade,
School of Electrical Engineering
Innovation Center of
the School of Electrical Engineering
Belgrade, Serbia

***Abstract*—In this paper we present a novel high-resolution algorithm for primary signal processing in High Frequency Surface Wave Radar (HFSWR). The high-resolution properties of the algorithm contribute to better ship detectability, as well as the ability to detect some ships, which are not visible at all using the currently used primary signal processing algorithms. The proposed algorithm is based on a high-resolution estimate of the range-Doppler map. We also proposed a numerically efficient Image Processing method for detection on the range-Doppler map. Azimuth estimation is performed by a high-resolution MUSIC-type algorithm that is executed for all targets detected on the range-Doppler map. The experimental results showed that the percentage of successful detections was high.**

***Index Terms*—HFSWR, OTHR, high-resolution methods, range-Doppler map, ship detection**

I. Introduction

High Frequency Surface Wave Radars (HFSWRs) are widely used for maritime surveillance of ships at long distances (up to 370 kilometers). Numerous published papers discuss theoretical as well as practical implementation aspects of HFSWR radars [1]- [3].

We have shown [4]- [6] that the multidimensional signal at the output of the dechirper can be modeled as a superposition of ionospheric interference, sea clutter, additive noise, and attenuated sinusoids (cissoids) in 3D space, i.e., fast-time, slow-time, and spatial domain. The domains correspond to the range, Doppler/radial velocity and azimuth of one target in a multi-target scenario, typical for HFSWRs, respectively. The first task of the proposed algorithm is to detect the number of superposed cissoids, i.e., the number of targets. The second task is to estimate the frequencies of these cissoids in the fast-time, slow-time, and spatial domain, which is equivalent to the estimation of their parameters (range, Doppler/radial velocity and azimuth).

Target detection performance depends on the chosen detection method. Constant False Alarm Rate (CFAR) detection methods are usually used in Frequency Modulated Continuous Wave (FMCW) HFSWRs, as explained in [7]. But some other detection methods like [8]- [11] are also proposed in the literature. CFAR detectors with adaptive treshold are widely used in HFSWR radars. In the paper we applied a kind of a detector which comes from image processing proposed by Natan [12]. The starting hypothesis of the authors was that such kind of detector is more suitable for detection in high resolution range-Doppler map than clasical CFAR. The reason for this is that propagation of noise in FFT-based range-Doppler estimation is predictable, but it is not predictable in high resolution methods. So, the question is if the optimal CFAR detector for detection in the classical RD-FFT map is also optimal for detection in the high-resolution RD-HR map. The other reason is that the applied image-based detector includes a kernel function, which can be optimised for specific shapes of taget lobes in RD-HR map and to improve target detectability. In the given application, we optimised the parameters of the applied detector (type of kernel, threshold levels, etc.) and compared the results with the results provided by a clasical CFAR detector. Furthermore, the nature of the MUSIC-based criterion function is more suitable for application of such kind of detectors, especially for close ranges in the RD-HR map.

Because target detection is still a challenging research problem, high-resolution methods for range/Doppler/azimuth estimation are in the focus of many scientific papers as presented in [13]- [15]. More detailed results of the research were presented in [16].

The paper is organized as follows. In Section II we presented the signal model. In Section III, we presented a detailed algorithm description: High-resolution range-Doppler map estimation (uniform/non-uniform sampling method in slow-time domain). In that section, we explained also the process of detection on the range-Doppler map, and an improved method for azimuth detection. We discussed some experimental results in Section IV and made some conclusions in Section V.

II. Signal model

The transmitter (Tx) and the receiver (Rx) array are synchronized in time and phase. The Tx transmits a periodic sequence of chirps at a carrier frequency f_c. The complex model of a single chirp, denoted by $c(t)$, is

This research was supported and APC was funded by Vlatacom Institute, Belgrade, Serbia. The research was also supported by the Serbian Ministry of Education, Science and Technological Development.

$$c(t) = e^{\mathrm{j}2\pi\psi(t)}, \quad t \in [0, T) \tag{1}$$

$$\psi(t) = \int_0^t f(\theta)\mathrm{d}\theta \tag{2}$$

$$f(t) = f_\mathrm{c} - \frac{B}{2} + \frac{B}{T}t, \tag{3}$$

where $\psi(t)$ is a phase function expressed in cycles and $f(t)$ is a frequency ramp, which yields

$$\psi(t) = \left(f_\mathrm{c} - \frac{B}{2}\right)t + \frac{B}{2T}t^2. \tag{4}$$

The transmit waveform, denoted by $r\left(\widetilde{t}\right)$, is then given by

$$r\left(t\right) = c(t), \quad 0 \le t < T \tag{5}$$

$$r\left(\widetilde{t}\right) = r\left(\widetilde{t} + T\right), \quad -\infty < \widetilde{t} < +\infty, \tag{6}$$

where $\widetilde{t}$ is a continuous time variable that spans the entire time-axis, whereas t is the time elapsed from the beginning of a chirp. We also define the index of a chirp, m, such that

$$\widetilde{t} = mT + t, \quad m \in \mathbb{Z}, \quad 0 \le t < T. \tag{7}$$

Note that the mutual dependence of the variables $\widetilde{t}$, t, and m is implied.

The signal reflected from the q-th target and then received by antenna n, $n \in \{1, 2, \ldots, N\}$, is

$$x_n^{(q)}\left(\widetilde{t}\right) = ar\left(\widetilde{t} - \tau_n^{(q)}\left(\widetilde{t}\right)\right) \tag{8}$$

$$\tau_n^{(q)}\left(\widetilde{t}\right) = \frac{2}{c}R\left(\widetilde{t}\right) + \tau_{\mathrm{A}n} \tag{9}$$

$$R\left(\widetilde{t}\right) \approx R_m + v_m t, \tag{10}$$

where $a \in \mathbb{R}$ is an attenuation factor, $\tau_n^{(q)}\left(\widetilde{t}\right)$ is the two-way propagation time for the target to antenna n, c is the radio wave propagation velocity, $R\left(\widetilde{t}\right)$ is the range to the target relative to the referent point of the Rx array, $R_m = R(mT)$, v_m is the radial velocity of the target during the m-th chirp (and is assumed constant during each chirp), $\tau_{\mathrm{A}n}$ is the delay at the n-th antenna relative to the referent point of the Rx array.

Instead of performing classical demodulation, the received signals are fed to a dechirper, which multiplies them by a conjugated replica of the Tx waveform. The signal at the output of the dechirper is given by

$$y_n^{(q)}\left(\widetilde{t}\right) = x_n^{(q)}\left(\widetilde{t}\right) r^*\left(\widetilde{t}\right). \tag{11}$$

In practical applications, we have that $0 < \tau_n\left(\widetilde{t}\right) \ll T$, so the end of the $(m-1)$-st chirp in $x_n\left(\widetilde{t}\right)$ and the beginning of the m-th chirp in $r\left(\widetilde{t}\right)$ overlap in only a small fraction of time. For other $\widetilde{t}$, the component of the dechirped signal corresponding to a stationary target is a simple cissoid. In the Rx, the received signal is given by

$$y_n\left(\widetilde{t}\right) = \eta_n\left(\widetilde{t}\right) + \sum_q y_n^{(q)}\left(\widetilde{t}\right), \tag{12}$$

where ionospheric interference, sea clutter and additive noise are modeled by $\eta_n\left(\widetilde{t}\right)$, and the sum is over all the targets. Finally, the dechirped signals are sampled at a rate f_s and fed to the algorithm.

III. Algorithm description

The samples are grouped into P-sample-long frames, where the length of each frame corresponds to the length of the chirp, T. Then, $M = 256$ successive frames are grouped into a segment. Adjacent segments overlap – the last 128 frames of a segment are the first 128 frames of the next segment. A segment is represented by a 3D matrix of samples $\mathbf{Y} \in \mathbb{C}^{M\times P\times N}$, whose elements are

$$y_{m,p,n} = y_n\left((m-1)T + (p-1)/f_\mathrm{s}\right), \tag{13}$$

for $1 \le m \le M$, $1 \le p \le P$, $1 \le n \le N$. Next, the elements of each row of $\mathbf{Y}$ are weighted by a Blackman-Harris window function, i.e. the row is multiplied element-by-element by $\mathbf{w}_P = [w_1, w_2, \ldots, w_P] \in \mathbb{R}^{1\times P}$. Then, the P-sample-long FFT (Fast Fourier Transform) is performed on each row (for each frame and each antenna) to obtain a matrix $\mathbf{S} \in \mathbb{C}^{M\times P\times N}$.

The WERA (WavE RAdar) primary signal processing is used as a benchmark. In WERA the next step is to perform weighting on each column of $\mathbf{S}$ by another Blackman-Harris window, $\mathbf{w}_M^\top = [w'_1, w'_2, \ldots, w'_M]^\top \in \mathbb{R}^{M\times 1}$, and perform M-sample-long FFT on it. As a result, a matrix $\mathbf{H} \in \mathbb{C}^{M\times P\times N}$ is formed. This matrix can be thought of as having the "Doppler", the "range", and the "antenna" dimension, and since it is obtained by FFT, we call $\mathbf{H}$ the RD-FFT (Range-Doppler) map. The next steps in WERA are the CFAR detection of targets in the RD-FFT map, followed by angle-of-arrival estimation for the detected targets using classical single-snapshot beamforming.

A. High-Resolution Range-Doppler Map Estimation – Uniform Sampling

The resolution of the RD-FFT map is limited by the resolution of the FFT, so we propose another algorithm to improve on this, with the following steps. We extend the matrix $\mathbf{S} = [s_{m,p,n}]$ by including the next $r(L-1)$ frames to get $\mathbf{S}' \in \mathbb{C}^{(M+r(L-1))\times P\times N}$, where r and L are algorithm parameters. We then form new matrices $\mathbf{Q}_{p,n} \in \mathbb{C}^{M\times L}$, $(\forall p, n)$, such that $\left[\mathbf{Q}_{p,n}\right]_{m,l} = \left[s_{m+r(l-1),p,n}\right]$, where $[\mathbf{A}]_{i,j}$ denotes the (i,j)-th element of $\mathbf{A}$. Then the covariance matrices $\mathbf{C}_{p,n} \in \mathbb{C}^{M\times M}$ are formed for $n = 1, 2, \ldots, N$ and $p = P - R + 1, P - R + 2, \ldots, P$ as follows:

$$\mathbf{C}_{p,n} = \frac{1}{L}\mathbf{Q}_{p,n}\mathbf{Q}_{p,n}^H, \tag{14}$$

where R is determined by the maximum radar range.

Since $\mathbf{C}_{p,n}$ is Hermitian positive definite, its eigenvalues are all positive. We propose to use a MUSIC-type algorithm, to get the RD-HR (High Resolution) map:

$$P_{\text{MUS}}^{\text{RD}}(\mu,p,n)=\frac{1}{\|\mathbf{a}_\mu(\mu)^{\text{H}}\mathbf{E}_{p,n}\|}, \tag{15}$$

where $\mathbf{E}_{p,n}\in\mathbb{C}^{M\times(M-K)}$ is the noise subspace matrix whose columns are the eigenvectors corresponding to the $M-K$ smallest eigenvalues of $\mathbf{C}_{p,n}$, where K is a parameter of the algorithm, and $\mathbf{a}_\mu(\mu)\in\mathbb{C}^{M\times 1}$ is a steering vector formulated in the normalized Doppler domain as

$$\mathbf{a}_\mu(\mu)=\left[1,\mathrm{e}^{-\mathrm{j}\mu},\ldots,\mathrm{e}^{-\mathrm{j}\mu(M-1)}\right]^\top, \tag{16}$$

where μ is the normalized Doppler frequency in radians per frame. The RD-HR map is calculated for a discrete set of points in the range of interest along each dimension, with a resolution that is many times better than the one of the RD-FFT map.

B. High-Resolution Range-Doppler Map Estimation – Non-Uniform Sampling

It was found that, in the uniform sampling method, the conditional number of the matrices $\mathbf{C}_{p,n}$ were in the order of 10^{19} (they were close to singular matrices), which created problems in their eigenvalue decomposition. The numerical complexity was also very high. To cope with these issues, we propose to use non-uniform sampling across the frames. This problem is analogous to selecting a small subset of antennas of an ULA, such that the performance of the array does not degrade significantly (a problem in the field of minimally redundant linear antenna arrays). Namely, we select a subset of J rows of the matrix $\mathbf{Q}_{p,n}$ by choosing an appropriate mapping $\ell:\{1,2,\ldots,J\}\to\{1,2,\ldots,M\}$, $J<M$. We then form $\mathbf{Q}_{p,n}^{(\ell)}$ as

$$\left[\mathbf{Q}_{p,n}^{(\ell)}\right]_{j,l}=\left[\mathbf{Q}_{p,n}\right]_{\ell(j),l}. \tag{17}$$

Thus, we get a much smaller covariance matrix

$$\mathbf{C}_{p,n}^{(\ell)}=\frac{1}{L}\mathbf{Q}_{p,n}^{(\ell)}\mathbf{Q}_{p,n}^{(\ell)\text{H}}\in\mathbb{C}^{J\times J}, \tag{18}$$

than the original $M\times M$ matrix $\mathbf{C}_{p,n}$. The criterion function is

$$P_{\text{MUS}}^{\text{RD}(\ell)}(\mu,p,n)=\frac{1}{\left\|\mathbf{a}_\mu^{(\ell)}(\mu)^{\text{H}}\mathbf{E}_{p,n}^{(\ell)}\right\|}, \tag{19}$$

where $\mathbf{E}_{p,n}^{(\ell)}$ is obtained from $\mathbf{C}_{p,n}^{(\ell)}$ in the same way $\mathbf{E}_{p,n}$ is obtained from $\mathbf{C}_{p,n}$ in the uniform sampling method and $\mathbf{a}_\mu^{(\ell)}$ is obtained from $\mathbf{a}_\mu$ by selecting the elements according to the same mapping ℓ.

C. Detection of Targets on the RD-HR map

An RD-HR map can be considered as a 2D image with its elements as the pixels. Targets are detected by finding the peaks in this map by adapted version of the detection algorithm proposed in [12]. However, to improve the performance, the map should first be filtered/smoothed to remove some of the interference.

It was found that the peaks of real targets have to span multiple pixels. Therefore, single-pixel peaks are false alarms and should be removed. To do this we apply the Median filter from the field of image processing. It is a kind of a nonlinear filter which selects a given pixel and its eight surrounding pixels and calculates their median as its output at the given pixel position. In other words, for a given map $\mathbf{P}\in\mathbb{R}^{M_\mathbf{P}\times P_\mathbf{P}}$, such as $\left[\overline{P}_{\text{MUS}}^{\text{RD}(\ell)}\right]$ or $\left[\overline{P}_{\text{MUS}}^{\text{RD}}\right]$, where $\overline{P}$ represents arithmetic mean of criterion function at all antennas, we select a 3×3 submatrix $\mathbf{M}(i,j)$ centered at (i,j) as

$$\mathbf{M}(i,j)=[\mathbf{P}]_{i-1:i+1,j-1:j+1}\ (\forall i,j), \tag{20}$$

where each edge of the map is padded with zeros, or more formally, $[\mathbf{P}]_{i,j}=0$, for all i,j where $i\in\{0,M_\mathbf{P}+1\}$ or $j\in\{0,P_\mathbf{P}+1\}$. $M_\mathbf{P}$ and $P_\mathbf{P}$ are lengths of RD-HR map by the Doppler and range dimension, respectively. Then the sub-matrix is rearranged into a vector, $\mathbf{m}(i,j)=\text{vec}\{\mathbf{M}(i,j)\}\in\mathbb{R}^{9\times 1}$, the vector is sorted which produces the vector $\mathbf{m}_\text{s}(i,j)$, and the resulting pixel is $[\mathbf{P}_\text{F}]_{i,j}=[\mathbf{m}_\text{s}(i,j)]_5$.

The second step is to apply a 2D linear FIR (Finite Impulse Response) filter to the map $\mathbf{P}_\text{F}$ to obtain $\mathbf{P}_\text{FF}$. Its impulse response (or kernel) can be thought of as a 7×7 matrix and is given by

$$\kappa(i,j)=\frac{1}{\sigma^2}\exp\left(-\frac{i^2+j^2}{2\sigma^2}\right);(\forall i,j\in\{-3,-2,\ldots,3\}). \tag{21}$$

The result is the convolution

$$[\mathbf{P}_\text{FF}]_{i,j}=\sum_{\zeta=-3}^{3}\sum_{\xi=-3}^{3}\kappa(\zeta,\xi)\,[\mathbf{P}_\text{F}]_{i-\zeta,j-\xi}, \tag{22}$$

where the edges of the map $\mathbf{P}_\text{F}$ are appropriately padded with zeros, i.e., $[\mathbf{P}_\text{F}]_{i,j}=0$, for all i,j where $i\in\{-2,-1,0,M_\mathbf{P}+1,M_\mathbf{P}+2,M_\mathbf{P}+3\}$ or $j\in\{-2,-1,0,P_\mathbf{P}+1,P_\mathbf{P}+2,P_\mathbf{P}+3\}$. Kernels of different sizes, such as 9×9, 5×5, or 3×3, can be used instead, but filtering with large kernels can be computationally demanding.

The next step after the filtering is to find peaks that exceed a chosen threshold γ. It is not a trivial task to choose a value for the threshold, since a lower value would improve the detection probability, but also increase the probability of false alarm. Also the signal from targets that are further away are usually weaker. Therefore, an adaptive threshold should be used.

D. Azimuth estimation for targets detected on the RD-HR map

After the detection of the peaks in the RD-HR map is performed, for each detected target, the same type of the criterion

function is calculated, but along the antenna dimension, to estimate the azimuth (angle of arrival). This method, with a 2D search followed by 1D search instances (one for each detection), has a much lower numerical complexity than the joint 3D search over the range-Doppler-azimuth domain. The steering vector in this case is

$$\mathbf{a}_\theta(\theta) = \left[1, \mathrm{e}^{-\mathrm{j}\nu}, \ldots, \mathrm{e}^{-\mathrm{j}\nu(N-1)}\right]^\top, \tag{23}$$

for a ULA, where $\nu = 2\pi f_\mathrm{c} d \sin\theta / c$, θ is the azimuth, and d is the distance between adjacent antennas.

If the peak of the q-th detected target is at (μ_q, p_q), then let $\mathbf{q}_{l,p_q,n}$ be the l-th column of $\mathbf{Q}_{p_q,n}$.

Doppler effect will be compensated using the vector $\mathbf{a}_\mu(\mu_q)$ and we get a scalar value as follows:

$$r_{n,l}^{(q)} = \mathbf{a}_\mu(\mu_q)^\mathrm{H}(\mathbf{q}_{l,p_q,n} \odot \mathbf{w}_M^\top). \tag{24}$$

Then we form the appropriate matrix

$$\mathbf{R}^{(q)} = \left[r_{n,l}^{(q)}\right] \in \mathbb{C}^{N\times L}. \tag{25}$$

In order for the detection to be better, we average the L covariance matrices and get one and continue with the algorithm for azimuth detection:

$$\mathbf{C}_\mathrm{A}^{(q)} = \frac{1}{L}\mathbf{R}^{(q)}\mathbf{R}^{(q)^\mathrm{H}} \in \mathbb{C}^{N\times N}. \tag{26}$$

The criterion function for the azimuth is

$$P_\mathrm{MUS}^\mathrm{A}(\theta, q) = \frac{1}{\left\|\mathbf{a}_\theta^\mathrm{H}(\theta)\mathbf{E}^{(q)}\right\|}, \tag{27}$$

where $\mathbf{E}^{(q)}$ is the noise subspace matrix of $\mathbf{C}_\mathrm{A}^{(q)}$.

The final estimate of the azimuth is determined by

$$\hat{\theta}^{(q)} = \arg\max_\theta \left|P_\mathrm{MUS}^\mathrm{A}(\theta, q)\right|. \tag{28}$$

IV. Experimental Results

The results presented in this section are based on the measured radar data, and their verification was made using Automatic Identification System data (AIS). A set of real signals (raw data) acquired on April 19, 2020 from the Over the Horizon Radar (OTHR) located on IBL location, Nigeria, in a time interval of 5 hours was used for testing.

The values $P = 1536$ and $N = 16$ are predefined. The first step in the proposed algorithm is to form an RD-HR map. We used the uniform sampling method. Here, we can see properties of range-Doppler maps and their main advantages and differences. The RD-HR map was calculated for Doppler frequencies from -0.4804 Hz to $+0.4804$ Hz to include the frequencies of ships of interest, as well as Bragg's lines. This range can be set arbitrarily. The range resolution was 375 meters.

RD-HR maps are formed for each antenna individually and independently. Target detection is performed on an averaged RD-HR map. In the second step, the azimuth is estimated using a high-resolution MUSIC-type algorithm, that is executed for each detection in the RD-HR map. Because of that, numerical complexity and the algorithm execution time are reduced. Angle resolution was chosen to be 0.2 degrees, and it is a much better resolution then the resolution used in many algorithms which are currently in use (typically 1 degree). Fig. 1 shows the complete detection process.

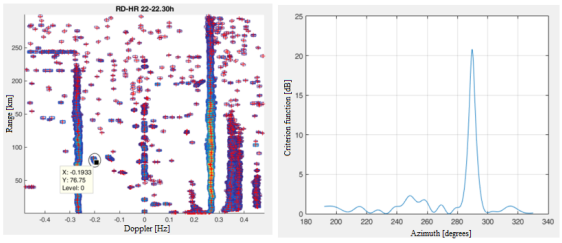

Fig. 1. Detection of vessel using the proposed algorithm: Detections in RD-HR map (left), Azimuth estimation for the selected vessel detected in RD-HR map (right)

As mentioned earlier, in a time interval of approximately 5 hours, we want to detect vessels using the proposed algorithm, and then compare the results with AIS data. Because of that, we made an experiment with 10 randomly selected vessels and monitored the detections throughout the time interval. The complete AIS data in a time interval of approximately 5 hours is plotted in Fig. 2a).

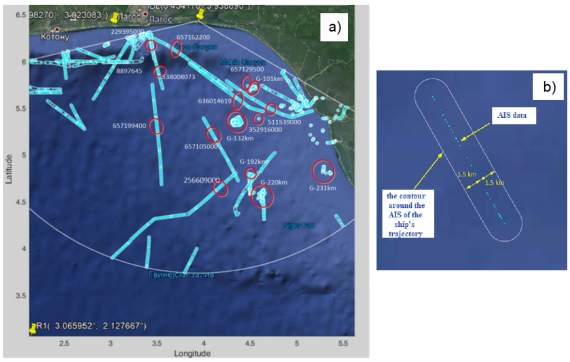

Fig. 2. a) The complete AIS data in a time interval of approximately 5 hours and randomly selected 10 vessels with their MMSI (Maritime Mobile Service Identity) identifiers and 5 stationary located groups of vessels with G identifiers b) A contour formed around the AIS data.

First, a contour is formed around the AIS data, where the width of the contour is equal to the size of the initial resolution cell of 1.5 km. Fig. 2b) illustrates the forming of the criterion contour.

Then the criterion was made so that the detections and AIS data are monitored for one hour, hour by hour. According to this criterion, if the detection is within the contour we will consider that a true detection and not a false alarm.

It can be noticed that in all cases the detections match the AIS data very well, and in the next step an accuracy analysis will be made depending on the selected algorithm

parameters (K and γ). Since we observe detections hour by hour, Fig. 3 shows an example of the appearance of detections on a geographic map from 17 pm to 18 pm for different values of algorithm parameters. Graphs of this type are very useful and can be used to monitor changes by the hour, for example if there is a change in climatic conditions, or if there is a change from day to night, etc.

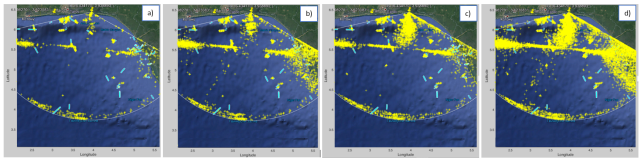

Fig. 3. The display of all vessel detections in a time interval of 1 hour (17-18 pm) for different detection parameters of the proposed algorithm: a) $K = 5$ and $\gamma = 0.2$ b) $K = 5$ and $\gamma = 0.1$ c) $K = 10$ and $\gamma = 0.2$ d) $K = 10$ and $\gamma = 0.1$

In the following analysis, the results of the detection of selected vessels will be presented in order to see the impact of certain parameters.

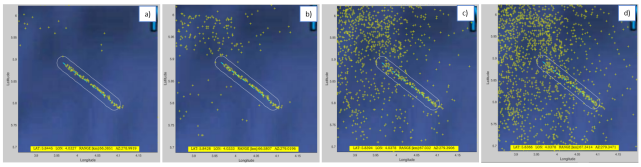

Fig. 4. The display of all detections of the vessel with MMSI=636014619 in a time interval of 1 hour (18-19h) for different detection parameters of the proposed algorithm: a) $K = 5$ and $\gamma = 0.2$ b) $K = 5$ and $\gamma = 0.1$ c) $K = 10$ and $\gamma = 0.2$ d) $K = 10$ and $\gamma = 0.1$

Fig. 4 shows detections for a vessel with MMSI=636014619 in a time interval of 1 hour (18-19h) for different detection parameters of the proposed algorithm. Tracks can be clearly seen and detections successfully follow the AIS data. The highest number of detections is in the case when the model number is higher and the detection threshold is lower. This certainly increases the detectability of vessels, but also increases the number of false alarms

The best performance is 76.67 % for chosen algorithm parameters K=10 and threshold 0.1. This clearly shows that the order of the model must be higher and the detection threshold lower in order for this percentage to be higher.

TABLE I
THE RATIO OF TOTAL NUMBER OF DETECTIONS AND NUMBER OF DETECTIONS WITHIN CONTOURS IN THE TIME INTERVAL OF 5 HOURS

Algorithm parameters	***In-contour***	***Non-contour***	***Ratio***
$K = 5, \gamma = 0.1$	7547	43186	6.7223
$K = 5, \gamma = 0.2$	6163	12732	3.0658
$K = 10, \gamma = 0.1$	10060	119044	12.833
$K = 10, \gamma = 0.2$	7610	44498	6.8473

An important parameter can be the ratio of true detections and total number of detections, as shown in Table I, and it is desirable that this number be as small as possible so that there are not too many false alarms.

V. CONCLUSIONS

In this paper, we presented new developed algorithm for primary signal processing in HFSWR and we discussed its properties. Based on the experimental results, the assessment of vessel detectability was made. We achieved great detectability in the selected time interval. The contributions are a high-resolution method for estimating the RD-HR map (a uniform and a computationally more efficient non-uniform variant), and the compensation of the Doppler shift before high-resolution azimuth estimation.The detection algorithm comes from the field of Image processing and it is, due to the kernel function, more convenient to use in the application of high-resolution methods than the classic CFAR, which is more suitable for use in FFT RDA map estimation.

REFERENCES

[1] K. Gurgel and T. Schlick, "Remarks on Signal Processing in HF Radars Using FMCW Modulation," Proceedings of the International Radar Symposium IRS 2009, Hamburg, Germany, 2009.

[2] M. Jankiraman, "FMCW Radar Design," Kindle ed., Artech House, England, 2018.

[3] A.M. Ponsford and J. Wang, "A review of high frequency surface wave radar for detection and tracking of ships," Turk J Elec Eng&Comp Sci, vol. 18, pp. 409–428, 2010.

[4] J.M. Headrick and M.I. Skolnik, "Over-the-Horizon Radar in the HF Band," Proc. IEEE, vol. 62, pp. 664–673, 1974.

[5] D.E. Barrick and J.B. Snider, "The Statistics of HF Sea-Echo Doppler Spectra," IEEE Trans. Antennas Propag., vol. 25, pp. 19–28, 1977.

[6] J. Sevgi, "Stochastic Modeling and Simulation Studies for the Surface Wave HF Radar: Problems and Challenges," 2003 Proceedings of the International Conference on Radar (IEEE Cat. No.03EX695), Adelaide, Australia, 2003.

[7] A. Dzvonkovskaya, K. Gurgel, H. Rohling and T. Schlick, "HF Radar WERA Application for Ship Detection and Tracking," J. Navig., vol. 7, pp. 18–25, 2009.

[8] A.L. Dzvonkovskaya and H. Rohling, "Adaptive thresholding for HF radar ship detection," Proceedings of Sixth Int. Radiowave Oceanography Workshop (ROW2006), Hamburg, Germany, 2006.

[9] Q. Li, W. Zhang, M. Li, J. Niu and Q.M. Jonathan Wu, "Automatic detection of ship targets based on wavelet transform for HF surface wavelet radar," IEEE Geosci. Remote Sens. Lett., vol. 14, pp. 714–718, 2017.

[10] S. Grosdidier and A. Baussard, "Ship detection based on morphological component analysis of high-frequency surface wave radar images," IET Radar Sonar Navig., vol. 8, pp. 48–53, 2012.

[11] J. Cai, H. Zhou, W. Huang and B. Wen, "Ship Detection and Direction Finding Based on Time-Frequency Analysis for Compact HF Radar," IEEE Geosci. Remote Sens. Lett., vol. 18, pp. 72–76, 2021.

[12] "Fast 2D peak finder," Available online: https://github.com/adinatan/fastpeakfind/releases/tag/1.13.0.0 (accessed on 20 Februry 2022).

[13] B. Kim, Y. Jin, J. Lee and S. Kim, "High-Efficiency Super-Resolution FMCW Radar Algorithm Based on FFT Estimation," Sensors 2021, vol. 21, 4018. https://doi.org/10.3390/s21124018, 2021.

[14] Y. Ji, J. Zhang, Y. Wang, G. Chang and W. Sun, "Performance Analysis of Target Detection with Compact HFSWR," Proceedings of 2016 CIE International Conference on Radar, Guangzhou, China, 2016.

[15] J. Xie, Y. Yuan and Y. Liu, "Super-Resolution Processing for HF Surface Wave Radar Based on Pre-Whitened MUSIC," IEEE J. Ocean. Eng., vol. 23, pp. 313–321, 1998.

[16] D. Golubović, M. Erić and N. Vukmirović, "High-Resolution Doppler and Azimuth Estimation and Target Detection in HFSWR: Experimental Study," Sensors 2022, vol. 22, 3558. https://doi.org/10.3390/s22093558, 2022.